Heliyon 10 (2024) e23605

Contents lists available at ScienceDirect

Heliyon

journal homepage: www.cell.com/heliyon

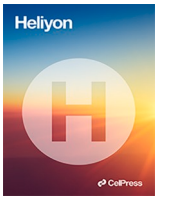

Cortical surface analysis for focal cortical dysplasia diagnosis by using PET images

Eric Jacob Bacon [a,b], Chaoyang Jin [a], Dianning He [a], Shuaishuai Hu [c], Lanbo Wang [d], Han Li [c,**], Shouliang Qi [a,b,*]

[a] College of Medicine and Biological Information Engineering, Northeastern University, Shenyang, China
[b] Key Laboratory of Intelligent Computing in Medical Image, Ministry of Education, Northeastern University, Shenyang, China
[c] Department of Neurosurgery, Shengjing Hospital of China Medical University, Shenyang, China
[d] Department of Radiology, Shengjing Hospital of China Medical University, Shenyang, China

ARTICLE INFO

Keywords:
Focal cortical dysplasia
Epileptogenic zone
FDG-PET
Cortical surface analysis
Machine learning

ABSTRACT

Focal cortical dysplasia (FCD) is a neurological disorder distinguished by faulty brain cell structure and development. Repetitive and uncontrollable seizures may be linked to FCD's aberrant cortical thickness, gyrification, and sulcal depth. Quantitative cortical surface analysis is a crucial alternative to ineffective visual inspection. This study recruited 42 subjects including 22 FCD patients who underwent surgery and 20 healthy controls (HC). For the FCD patients, T1-weighted and PET images were obtained by a PET-MRI scanner, and the confirmed epileptogenic zone (EZ) was collected from postsurgical follow-up. For the HCs, CT and PET images were obtained by a PET-CT scanner. Cortical thickness, gyrification index, and sulcal depth were calculated using a computational anatomical toolbox (CAT12). A cluster-based analysis is carried out to determine each FCD patient's aberrant cortical surface. After parcellating the cerebral cortex into 68 regions by the Desikan-Killiany atlas, a region of interest (ROI) analysis was conducted to know whether the feature in the FCD group is significantly different from that in the HC group. Finally, the features of all ROIs were utilised to train a support vector machine classifier (SVM). The classification performance is evaluated by the leave-one-out cross-validation. The cluster-based analysis can localize the EZ cluster with the highest accuracy of 54.5 % (12/22) for cortical thickness, 40.9 % (9/22) and 13.6 % (3/22) for sulcal depth and gyrification, respectively. Moderate concordance (Kappa, 0.6) is observed between the confirmed EZs and identified clusters by using the cortical thickness. Fair concordance (Kappa, 0.3) and no concordance (Kappa, 0.1) is found by using sulcal depth and gyrification. Significant differences are found in 46 of 68 regions (67.7 %) for the three measures. The trained SVM classifier achieved a prediction accuracy of 95.5 % for the cortical thickness, while the sulcal depth and the gyrification obtained 86.0 % and 81.5 %. Cortical thickness, as determined by quantitative cortical surface analysis of PET data, has a greater ability than sulcal depth and gyrification to locate aberrant EZ clusters in FCD. Surface measures might be different in many regions for FCD and HC. By integrating machine learning and cortical morphologies features, individual prediction of FCD seems to be feasible.

* Corresponding author. College of Medicine and Biological Information Engineering, Northeastern University, Shenyang, China.
** Corresponding author.
E-mail addresses: baconbacon205@outlook.com (E.J. Bacon), 1136624725@qq.com (C. Jin), hedn@bmie.neu.edu.cn (D. He), shuai_hu@yeah.net (S. Hu), rambo0808@163.com (L. Wang), leoincmu@gmail.com (H. Li), qisl@bmie.neu.edu.cn (S. Qi).

https://doi.org/10.1016/j.heliyon.2023.e23605
Received 31 May 2023; Received in revised form 14 October 2023; Accepted 7 December 2023
Available online 12 December 2023

1. Introduction

Focal cortical dysplasia (FCD) is a disorder marked by faulty development of a single portion of the brain's outer layer, generally known as the cerebral cortex. This disorder is a prevalent cause of epilepsy, particularly in children, young adults, but also in adults [1]. A complete history and physical examination are frequently used to make the diagnosis of FCD. The majority of FCD cases linked with seizures are drug-resistant. In such circumstances, individuals should be examined for resective epilepsy surgery, which has the potential to greatly reduce seizure load or perhaps lead to seizure freedom [2]. FCD is classified into three types (Type I, Type II, and Type III). According to the most recent International League Against Epilepsy (ILAE) classification, FCD Type I is a histological category distinguished by architectural disorder of the neocortex as a result of impaired developmental maturation and the absence of any other primary epileptogenic lesion in the brain (as validated by MRI or histopathology). Whereas, FCD Type II is characterized by mild defects in cortical development and accounts for 9 % of all cases in epilepsy surgical case series, with the frontal lobe accounting for 51 % of histopathological proven cases. This kind of FCD is frequently linked to drug-resistant epilepsy. FCD Type III is characterized by abnormal neocortical architectural organization in the vicinity of epileptogenic lesions such as hippocampal sclerosis, developmental brain tumours, vascular malformations, or any other early-life lesion such as pre- or perinatal infarction, bleeding, or inflammation. It should be noted that each of these categories of FCD is further classified into different types [3].

Despite recent advances in neuroimaging, diagnosing FCD remains difficult. The vast majority of Type II cortical dysplasia cases exhibit abnormalities magnetic resonance imaging (MRI), whereas the vast majority of Type I cases do not. FCD are small or inconspicuous, making them difficult to detect visually on an MRI. Histopathological MRI studies show that during ocular inspection, approximately 40 % of Type II FCD are negative, but approximately 85 % of Type I FCD are negative [4,5]. This statistic varies according to the imaging technique and the interpreter's level of competence. additional imaging techniques such as FDG-PET (Fluorodeoxyglucose-positron-emission-tomography) are described as a useful alternative in diagnosing abnormalities for FCD [6]. FDG-PET can be used to help identify seizure disorders, which can help identify occult lesions on MRI data. It is frequently used to detect focal hypo-metabolism in the FCD regions with a diagnostic sensitivity for FCD detection estimated at 78–83 % [7,8]. This sensitivity is further enhanced using simultaneous PET/MRI recording [9,10]. Though FDG-PET appears to have higher sensitivity in diagnosing than MRI, visual assessment has various limits and several uncertainties in the method. Visually interpreting FDG-PET data relies on human observers' subjective interpretation of the images, which largely focuses on qualitative interpretation but does not provide accurate quantitative measures or objective criteria for diagnosis [11,12]. For the reasons mentioned above, an additional analysis procedure is needed to provide an accurate diagnosis. Therefore, the advantages of quantitatively combining multiple modalities with PET for FCD detection merit further exploration.

To analyse FCD, several alternatives to visual assessment are used. Voxel-based morphometry (VBM) is one of these, a regularly used approach for assessing drug-resistant epilepsy. We previously utilised this approach [11] to evaluate individuals with refractory epilepsy by identifying the epileptogenic zone(EZ). Riney et al. examined children with epilepsy using VBM on FLAIR (Fluid--attenuated inversion recovery) MRI images [12]. Although prior studies have discovered cortical anomalies in FCD patients, the results have not been consistent, which could be attributed to variances in the specific patient samples analysed or the methodologies utilised. Cortical morphologies were discovered to reflect intermediate progenitor cell regulation creation and amplification in the current study [13].

Surface-based analysis can also aid in the assessment and diagnosis of cortical morphology. Thesen et al. use an automated, surface-based method for evaluating morphometric characteristics associated with cortical epileptogenic anomalies to detect aberrant thickness in the cortical surface and blurring grey-white matter boundaries [14]. Spitzer et al. built an open-source, interpretable surface-based machine-learning system to detect FCDs in heterogeneous structural MRI data from epilepsy surgical centers throughout the world [15]. Cortical morphological investigations, such as cortical thickness, are commonly employed to study the neuroplastic alterations associated with pathophysiological changes and abnormalities. Moreover, sulcal depth and gyrification, two morphological metrics that parallel cortical thickness, have received less attention in FCD research [16]. Deep sulcal areas have a relatively stable spatial distribution and are responsive to cortical development and atrophy [17,18]. The cerebral gyrification properties adapt the cortical surface area to the geometry of the skull, enhancing neural circuit development [19]. As a result, the cortical morphology examination may contribute to more rigorous and reliable information on the underlying neurophysiological mechanisms driving FCD.

Therefore, the purpose of this study is to implement a thorough examination of cortical morphological development utilising FDG-PET imaging, and to look at the relationships between cortical abnormalities in FCD patients [20–22]. Based on past FCD neuroimaging research investigations [23–25], we hypothesized that cortical characteristics would reveal major metabolic abnormalities or aberrant activity in FCD-affected regions. However, we intend to use PET-MRI and PET-CT in our investigation because we believe that quantitatively analysing them could potentially improve the identification of abnormal activity in the brain. Furthermore, we hypothesized that the main alterations observed in the cortical surfaces of FCD patients were due to fluctuations in the strength of these features [26,27].

To test these ideas, the cortical morphologies will be quantitatively examined using CAT12, a volumetric analysis tool supplied by SPM that provides a quick and simple alternative method for cortical surface analysis. CAT12 has demonstrated high sensitivity in studies of neurological illnesses such as refractory epilepsy and epileptogenic zone localisation [11]. It is used to determine the cortical thickness, sulcal depth, and gyrification index. A cluster-based analysis is carried out to determine each FCD patient's aberrant cortical surface. To evaluate whether the characteristic in the FCD group had altered significantly, a region of interest (ROI) analysis was done. Finally, all ROI features were trained in a machine learning classifier to distinguish FCD from healthy controls.

2. Materials and methods

2.1. Participants

The dataset for the current study initially comprised 50 people (25 patients with FCD and 25 healthy controls (HC)). The populations in the dataset were all subjected to a selection criterion, such as image quality and age. The technique and selection criteria are depicted in Fig. 1.

The study finally, included 42 participants, including 22 patients and 20 healthy controls. The patients' average age and standard deviation (SD) are 31.9 ± 11.8 years, with 68.2 % (15/22) males and 31.8 % (7/22) females. The healthy controls had a mean age and standard deviation of 25.8 ± 7.7 years, with 42.9 % (8/20) males and 57.1 % (12/20) females. From January 2018 to July 2019, patients were subjected to pre-surgical investigation at the Shengjing Hospital of China Medical University, Shenyang, China. A full clinical history and neurological examination were performed, as well as a complete cognitive assessment, psychiatric assessments. It also contained long-term scalp video-EEG, MRI, and PET data for inter-ictal and ictal onset sequence. The scanned images were taken in accordance with the clinical routine of epilepsy for both patients and healthy controls. The Ethics Committee of Shengjing Hospital of China Medical University approved this study. All participants in the experiment signed an informed consent form, consented to have the MRI images published, and were informed about the study methodology.

All 22 patients had medically resistant epilepsy surgically removed, with histological confirmation of FCD. Specialists analysed the pathology of the specimen and subtyped it using the ILAE categorization [28]. Presurgical examination information on the patients' seizure onset zones, age, and gender and pathological subtype of FCD are presented in Table 1. All patients are in Type II. The Engel value was used to evaluate the surgical results of all patients, and the result was validated by the postsurgical follow-up EZ. Six months following the procedure, the Engel value was evaluated.

2.2. FDG-PET images acquisition

Regardless of whether the study was conducted on patients or a control group, all PET imaging scans were obtained and analysed in accordance with clinical epilepsy methods. A GE Healthcare SIGNA PET/MR scanner (Waukesha, WI, USA) is used to acquire images of patients. Subjects were instructed to relax silently for 45–60 min following intravenous administration of 3.7 MBq/kg of 18 F-FDG. To reconstruct PET scans, the standard 3D ordered subsets expectation maximisation (OSEM) technique (32 subsets and three iterations) is employed. The restored data has a 192 × 192 × 16 matrix and a voxel scale of 1.56 × 1.56 × 2.40 mm^3. Each scan takes roughly 15 min to acquire.

The images of the healthy control group were taken using a Discovery 690 PET (General Electric) from Shengjing Hospital of China Medical University. After receiving 5 MBq/kg of 18 F - FDG intravenously, the subjects were advised to relax silently in a dimly lit room for around 40 min. A standard 11-min method is employed to obtain projection data for 25 tomographically corrected attenuation-corrected images brain areas with a thickness of 3.27 mm. The mode helical was employed with a restoration width of 700 mm and a slope for rescale of 1.0. The PET data was restored using the OSEM technique, which had 16 subsets and six iterations. Finally, the reconstructed matrix data is 512 × 512 × 16 with a voxel scale of 3.65 × 3.65 × 3.27 mm^3.

2.3. MRI and CT acquisitions

To acquire the MRI images, a GE Healthcare SIGNA PET/MR scanner (16-channel head coil) was employed. The following sequences were included in the protocol: Sag 3D T1BRAVO (T1w; TE = 3.3 ms, flip angle = 12°, TR = 8.5 ms, voxel size = 0.469 × 0.469 × 1 mm^3 matrix size = 512 × 512, the Magnetic Field Strength = 3.0 T). The subjects were advised to remain awake while closing their

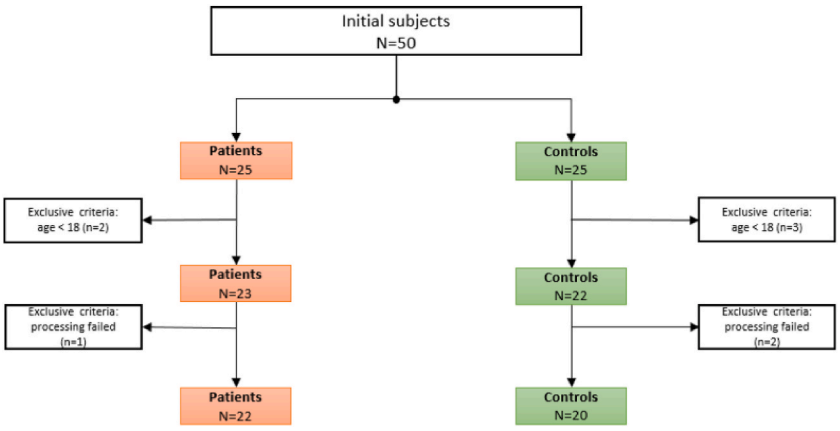

Fig. 1. Criteria and the procedure for selecting subjects.

Table 1
Presurgical examination information on the patients' seizure onset zones, age, and gender and pathological subtype of focal cortical dysplasia.

Patient	Seizure onset zone	Abbreviation	Age (year)	Gender	Type
1	Right medial temporal lobe structure	R\mT	48	F	Type I
2	Right medial temporal lobe structure	R\mT	27	M	Type I
3	Left medial temporal	L\mT	21	M	Type I
4	Right medial temporal lobe structure	R\mT	35	M	Type I
5	Medial lateral right temporal lobe	R\mT	34	F	Type I
6	Right medial temporal lobe structure	R\mT	35	M	Type I
7	Right medial temporal lobe structure	R\mT	24	M	Type I
8	Left medial temporal lobe structure	L\mT	28	M	Type I
9	Left frontal	L\F	38	F	Type I
10	Left middle temporal	L\mT	45	M	Type I
11	Left middle temporal	L\mT	28	M	Type I
12	Left middle temporal	L\mT	35	M	Type I
13	Left middle temporal	L\mT	38	M	Type I
14	Left middle and lateral temporal	L\m & laT	16	F	Type I
15	Hippocampus, right temporal lobe	R\mT	22	F	Type I
16	Left medial temporal lobe	L\mT	27	M	Type I
17	Left temporal lobe	L\T & L\mT	23	F	Type I
18	Right temporal occipital lobe	R\T & R\O	26	M	Type I
19	Right parietal lobe	R\P	12	F	Type I
20	Left middle temporal (Hippocampus)	L\mT	32	M	Type I
21	Right frontal	R\F	24	M	Type I
22	Left medial temporal lobe structure	L\mT	24	M	Type I

eyes and lying down for the subsequent tests. Slices were inclined in an oblique axial position to help reduce signal losses and warp in the mesiotemporal and orbitofrontal areas.

The CT scan was obtained at Shengjing Hospital of China Medical University using a Discovery 690 CT (General Electric). The following are the acquisition parameters: The slice thickness is 3.75 mm, with a slice spacing of 3.27 mm. The scan mode is helical, with a restoration diameter of 500 mm and a slope for rescale of 1.0. Finally, the reconstructed matrix data is $512 \times 512 \times 16$ with a voxel scale of $3.65 \times 3.65 \times 3.27$ mm^3, and a resolution of 140 kVp.

2.4. Data processing

The processing method of our study consisted of three steps which involve data pre-processing, data processing, and statistical analysis as shown in Fig. 2.

During the data pre-processing step, all images, including PET and T1W, were converted to the Nifti format [29] from the original Dicom format [28]. Then, PET scans were registered to the canonical template and realigned. Finally, the PET scans were co-registered with the T1W images.

CAT12 was employed to carry out the cortical surface analysis on our data during the processing step. This innovative fully automated approach based on projection-based thickness (PBT) was utilised to measure cortical thickness and the core surface of the cortex in a single step [30,31]. The images were automatically segmented into three volume tissues (grey matter (GM), white matter (WM), cerebrospinal fluid (CSF)), and several other cortical tissues. Following segmentation, the segmented features were automatically affine registered to MNI template space and nonlinearly deformed.

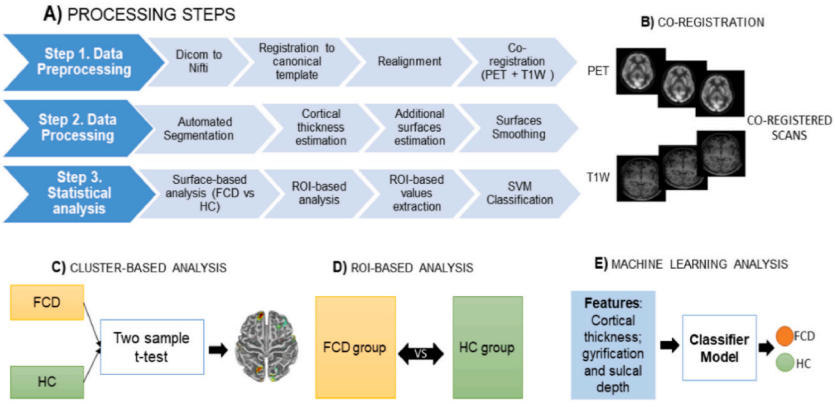

Fig. 2. Flowchart of the study procedure. **(A)** Processing steps; **(B)** Co-registration. **(C)** Cluster-based analysis. **(D)** ROI-based analysis. **(E)** Machine learning analysis.

The thickness was then retrieved using the PBT approach, which employs a projection system that takes into account blurring sulci to get an accurate cortical thickness map [32]. The PBT method estimates the WM distance using tissue segmentation and then projects the local maximum (This is comparable to the thickness) to neighbouring GM voxels are connected using a neighbour connection determined by the WM distance.

Several additional surface measurements were retrieved, including the sulcal depth (SuD) and gyrification index (GI). The GI is determined using absolute mean curvature and is expressed as a proportion of the external brain surface to the outside surface after the sulci are removed. Sulcus depth is calculated using the Euclidean distance betwixt the centre surface and its convex hull. The square root-transformed sulcus depth is used in this case because the function of the square root is used to make the data more consistently distributed [30].

The recently produced surfaces were smoothed with various Gaussian smoothing kernel values, namely 15 mm FWHM for thickness and 20 mm for GI and SuD. Three sections are included in the statistical analysis process, i.e., the cluster-based, ROI-based, and machine learning-based analysis.

2.5. Cluster-based analysis

Cluster-based analysis was first conducted. For each surface feature (thickness, GI and SuD), a two-sample *t*-test is conducted between each FCD patient and HC group using age as the covariate. The clusters showing significant changes in the surface measure of a single FCD patient will be obtained.

In our study, we defined a cluster as a group of vertices on the cortical surface. A significant cluster is obtained when the cluster size is above 100 mm^3. A brain region is declared to be abnormal if a cluster is identified within it. One or more abnormal regions can be identified for a single patient. When more regions are identified, the region with the highest intensity peak (T-value) will be considered the main region identified for the patient. If this region matches the postsurgical confirmed EZ, a correct finding is achieved for this patient. An accuracy score can be determined for all the patients.

The abnormal brain regions identified from the cluster-based analysis are compared with the postsurgical confirmed EZ by Cohen's kappa statistical test. To facilitate the comparison, the abnormal brain regions were grouped into 4 lobes (parietal, frontal, occipital, and temporal) in each hemisphere according to match the postsurgical follow-up EZ reports. The following is how the relationship between Kappa value (k) and agreement level is interpreted: When $k = 0$, there is no agreement; when $k = 0.01–0.20$, there is no or slight agreement; when $k = 0.21–0.40$, the agreement is fair; when $k = 0.41–0.60$, the agreement is moderate; when $k = 0.61–0.80$, the agreement is substantial; and finally, when $k = 0.81–1.00$, the agreement is almost perfect. SPSS version 22.0 software (IBM-SPSS, Armonk, NY, USA) was used for all statistical analyses.

2.6. The ROI-based analysis

ROI-based analysis was also performed using the extracted surface measures. The ROI was defined using the Desikan-Killiany atlas, and 68 cortical regions (34 per hemispheres) in total were extracted [33]. The thickness, GI, and SuD of each ROI were calculated for each FCD patient and HC. A two-sample test was used for each ROI measure to determine the statistical significance between the FCD and HC groups. Moreover, for a measure of all ROIs, the Spearman correlation analysis was conducted between FCD and HC groups. If $p < 0.05$, a significant correlation is available; otherwise, they are independent of each other [34].

2.7. Machine learning-based analysis

Finally, the 68 ROI features extracted were assessed using a machine learning classifier to differentiate FCD from HC. The support vector machines (SVM) classifier was employed to complete the classification task, with the post-surgical confirmed EZ used as the ground truth. For the prediction tasks, 10-fold cross-validation is used to assess classification performance. Here, k-fold cross-validation has been considered one comprehensive way for predictive model evaluation [35]. The goal is to make the best use of our training data to estimate the achievement of a model on unseen data. The model's accuracy and sensitivity were also estimated.

3. Results

3.1. The identified potential EZ clusters

Table 2 presents the demographic data of participants. For cortical thickness, abnormal clusters were identified in all FCD patients,

Table 2
Demographic information.

Characteristics	Patients	Healthy Controls
Number of patients	22	20
Gender (male/female)	15/7	8/12
Age (years)	15–63	15–48
(Mean ± SD)	31.9 ± 11.8	25.8 ± 7.7

indicating a positive finding rate of 100 %. Gyrification and sulcal depth showed the same positive finding rate of 95.5 %. Table 3 displays clusters of patients with significant alterations in thickness, GI, and SuD (No. 8). For the thickness, the cluster with the largest size is located in the left insula and it also has the highest T-value of 6.06. Cortical thickness has more aberrant regions than gyrification and sulcal depth.

Fig. 3 shows an example of the identified abnormal clusters for three different patients (No. 03, 07, 20). Each column highlights the finding of specific cortical features, while each row describes the outcome of a single patient. The cluster with the largest cluster size and the highest T-value peak is chosen as the most significant EZ. The cortical thickness output more visible clusters than others that showed subtle clusters. As an example, for patient 03 (P03), the most significant clusters were shown in the left frontal and occipital for the cortical thickness. The same observation was made for patients 07 and 20 (P07 and P20).

Table 4 shows the comparison of the two-sample *t*-test outcomes to the confirmed EZ for all the patients. Cortical thickness correctly identified 54.5 % (12/22) of patients, followed by sulcal depth and gyrification, which correctly identified 40.9 % (9/22) and 13.6 % (3/22) of patients, respectively. There are six overlapped regions between those detected by cortical thickness and sulcal depth, but only two overlapped regions between thickness and gyrification and four overlapped regions between gyrification and sulcal depth.

3.2. Concordance between possible and verified EZ clusters

Cohen's kappa statistic for the cluster-based analysis yielded different results across three measures. The identified potential EZ clusters and the confirmed EZs yielded a moderate concordance for the cortical thickness ($k = 0.6$), while a fair concordance is obtained for the sulcal depth ($k = 0.3$), and no concordance is found for the gyrification ($k = 0.1$).

3.3. Differences in surface measures between FCD and HC

The ROI-based analysis reveals statistically significant differences in 46 out of 68 (67.7 %) cortical regions between FCD and HC populations, as illustrated in Fig. 4. It provides an overview of ROI-based analysis in terms of the cortical thickness (Fig. 4(A)), the gyrification (Fig. 4(B)), and the sulcal depth (Fig. 4(C)). Fig. 4(D) highlights the brain regions exhibiting diverse ROIs and statistically significant variations in the thickness, GI, and SuD.

Among the 46 regions, 22 were located in the left hemisphere with some of them in the inferior temporal gyrus, precuneus gyrus, para-hippocampal gyrus, middle frontal gyrus, and posterior-cingulate gyrus. The right hemisphere identified 24 regions (Middle temporal, anterior cingulate, hippocampal, occipital, and superior frontal). The same observation was made for all three surface measures. In addition, the spearman correlation yielded a high p-value (0.06, 0.07 and 0.06) for the cortical thickness, gyrification and sulcal depth.

3.4. Individual prediction of FCD

The SVM classifier has a prediction accuracy of 95.5 % for cortical thickness, and 86.0 % and 81.5 % for sulcal depth and gyrification, respectively. Fig. 5 illustrates the receiver's operating characteristics with its area under the curve (ROC-AUC), whereas Fig. 6 depicts the confusion matrix of the classifiers. The cortical thickness yielded a sensitivity of 96.0 % for gyrification, while the sulcal depth and cortical thickness obtained 95.0 % and 88.0 % respectively. 21 out of 22 (95.0 %) patients and 19of 20 (95.0 %) HCs are predicted correctly for the cortical thickness. The gyrification correctly predicted 20 out of 22 (90.9 %) patients and 14 out of 20 (70.0) HCs. The sulcal depth correctly predicted 18 out of 22 (81.8 %) patients and 18 out of 20 (90.0 %) HCs.

4. Discussion

In our study, surface-based analysis was used to analyse PET images for FCD diagnosis. The study provides new information on the

Table 3
Abnormal clusters with major changes in the cortical morphology of a single FCD patient (e.g., No. 8).

Hemispheres/cortical morphology	Location	Cluster size	T value	MNI'		
				X	Y	Z
Thickness						
LH	Insula	7500	6.06	−36	−23	0
	Superior temporal	104	3.11	−64	−32	10
	Inferior temporal	202	3.08	−52	−15	−32
RH	Frontal	200	2.52	13	66	6
Gyrification						
LH	Cingulate	421	2.62	−3	−49	27
	Lingual	204	2.53	−26	−56	−8
RH	–	–	–	–	–	–
Sulcal Depth						
LH	Lingual	2188	3.18	−12	−70	−8
RH	–	–	–	–	–	–

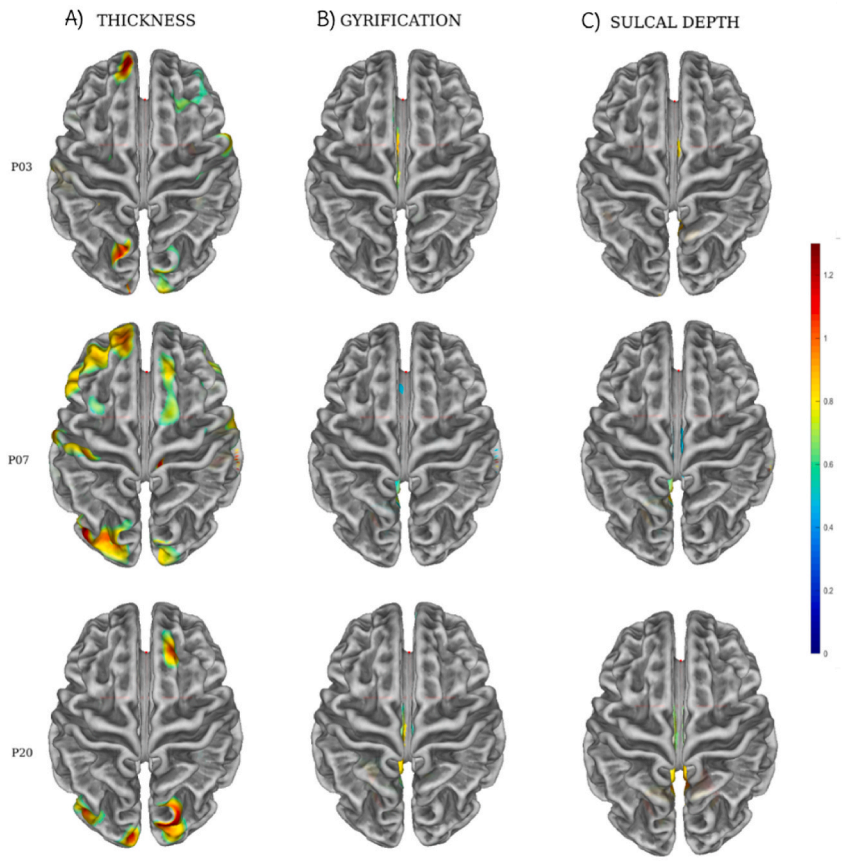

Fig. 3. Illustrations of detected aberrant clusters in three distinct patients (e.g., Patient Numbers: 03, 07, 20). The first row presents the findings for Patient 03, while the second row exhibits results for Patient 07, and the third row highlights the outcomes for Patient 20. Each column corresponds to a specific cortical characteristic, with the first column representing the cortical thickness (A), the second column illustrating the gyrification (B), and the third column depicting the sulcal depth (C).

relationship between cortical area measurements and FCD. Firstly, the cluster-based analysis successfully identified abnormal clusters in FCD (Thickness). Secondly, the ROI-based analysis showed the differences between the FCD and HC populations. Finally, the trained SVM classifier achieved a good prediction accuracy the sulcal obtained the highest prediction score.

4.1. Main findings and their significance

The cortical thickness identified the highest number of clusters during the cluster-based analysis, while the other two features identified less. These observed differences during our analysis might be explained by the tissue characteristics of each cortical measurement [14]. Cortical thickness and gyrification present different characteristics, this assertion is confirmed by Gautam et al. [36]. Cortical gyrification is substantially and favourably associated to the cerebral cortex (cortical volume), but adversely associated to the thickness in several parts of the cortex, according to the authors.

Frontal gyrification has also been associated to improved short-term memory and cognitive flexibility [37]. This assumption could explain the disparity reported between the results of cortical thickness and gyrification. On the contrary, Tosun et al. found some parallels between thickness and SuD [38]. The authors established that aberrant pre- and post-central relationships between CThick and SDepth in children with partial epilepsy could be a biomarker of mental comorbidity. Another factor that could explain the observed discrepancy in cortical thickness and sulcal depth is the smoothing kernel size. The cortical thickness in our study is 15 FWHM, while the sulcal depth is 20 FWHM [14].

The results of the ROI-based analysis can support the assumption that illness patients have basic disparities in brain structural measurements. Dworkin et al. studied this topic and effectively addressed a strategy for finding local group variations in multivariate density at the subject-level [39]. Another reason could be the structural differences between the two PET modalities. This claim was corroborated by Mayerhoefer et al. According to the authors, PET/MRI provides for more appropriate care than PET/CT in minimal proportion of cancer sufferers [40].

Our study also explores a machine learning analysis to do individual predictions based on the cortical morphologies extracted. The machine learning analysis performed well. The observed prediction outcomes proved that integrating machine learning in

Table 4
Comparison between cluster-based analysis outcomes and postsurgical confirmed EZs.

Subject	Thickness	Gyrification	sulcal Depth	EZ
1	L/T	L/T	L/T	L/F
2	R/T	L/O	R/F	R/MT
3	L/F	R/F	L/T	L/MT
4	R/O	L/O	R/T	R/MT
5	L/O	R/F	R/T	R/MT
6	L/T	R/T	L/T	R/MT
7	L/T	R/T	R/O	R/MT
8	L/T	R/T	L/O	L/MT
9	L/F	L/O	L/T	L/F
10	L/O	R/F	R/T	R/MT
11	L/T	L/O	L/T	L/MT
12	L/T	L/O	L/T	L/MT
13	L/T	L/O	L/P	L/MT
14	R/P	none	R/P	R/P
15	L/T	L/T	R/O	L/MT
16	L/T	L/O	L/O	L/MlT
17	R/P	L/O	none	R/MT
18	L/T	L/O	L/T	L/MT
19	L/T	R/T	R/T	R/TO
20	R/O	L/O	L/O	R/P
21	L/T	R/F	R/T	L/MT
22	R/F	L/O	R/T	R/F

L stands for left hemisphere, R stands for right hemisphere, F stands for frontal, T stands for temporal, O stands for occipital, P stands for parietal, M stands for middle, and l stands for lateral.

neurological disease, might bring more facilities in the way of analysing neuroimaging data and may help in diagnosing FCD more accurately. Previous studies have shown that machine learning can outperform human capacities in many fields including neuroimaging. This assertion is supported by Varoquaux et al., who uncovered new aspects of the cognitive organization using their machine learning model and performed well [41]. Hence, integrating quantitative and machine learning analysis might contribute a lot and become a crucial alternative to the visual assessment of FCD [14,42,43].

4.2. Why are cortical thickness, gyrification, and sulcal depth utilised in FCD diagnosis?

Diagnosing FCD remains challenging for medical scientists since the visual inspection is ineffective with a lot of inconsistencies. The purpose of this study is to provide additional technique to diagnose FCD. To fulfil the study's goal, we recommend assessing the thickness, GI, and SuD. Several researchers studied the efficacy of cortical parameters such as thickness, GI, and SuD in assessing epilepsy patients. Sophie et al. addressed the constraints of a paediatric population by developing an automated technique for FCD detection based on cortical thickness and gyrification characteristics [44]. Tosun et al., evaluated the cortical (CThick-SDepth) relationship between normally growing children and those with focal epilepsy (TDC) [38]. MRI-negative images include enough information to help detect visually ambiguous FCD in vivo. Ahmed et al. described a quantitative morphometry strategy for distinguishing FCD lesions in MRI-negative candidates that incorporates machine learning algorithms and surface-based MRI processing techniques. Their method found much more MRI-negative individuals with lesions, and the classification task was effective, with 14 of 24 FCD lesions properly identified (58 %) [45].

4.3. CAT12 performance for cortical surface analysis

The computational anatomy toolbox is a volumetric toolbox that provides a quick and simple alternative method for cortical surface examination. Several academics have attempted to compare its performance to that of existing tools. Seiger et al. compared the CAT12 toolbox's performance to that of FreeSurfer. Their investigation discovered that CAT12 outperformed FreeSurfer and provided additional proof that the toolbox produces precise and profitable results [31]. Though FreeSurfer will most certainly remain a mainstay for thorough cortical morphology assessments, CAT12 appears to be a solid alternative that might be very useful for research scientists or physicians. Righart et al. attempted to validate CAT12 in comparison to FreeSurfer [46]. Li et al. used CAT12 cortical morphometry to examine changes in SuD, GI, and thickness of Codeine-containing cough syrup (CCS) users' cerebral cortex. Their findings were encouraging due to significant changes in SuD, GI, and thickness [47].

4.4. The significance of machine learning in the detection of FCD

Several studies have used machine learning to explore FCD. Demerath et al. recently published a study to see if the detection of FCD can be improved further by feeding this approach magnetization-prepared two rapid acquisition gradient echoes (MP2RAGE) datasets instead of magnetization-prepared rapid acquisition gradient echo (MPRAGE) datasets [48]. Ganji et al. assessed cortical

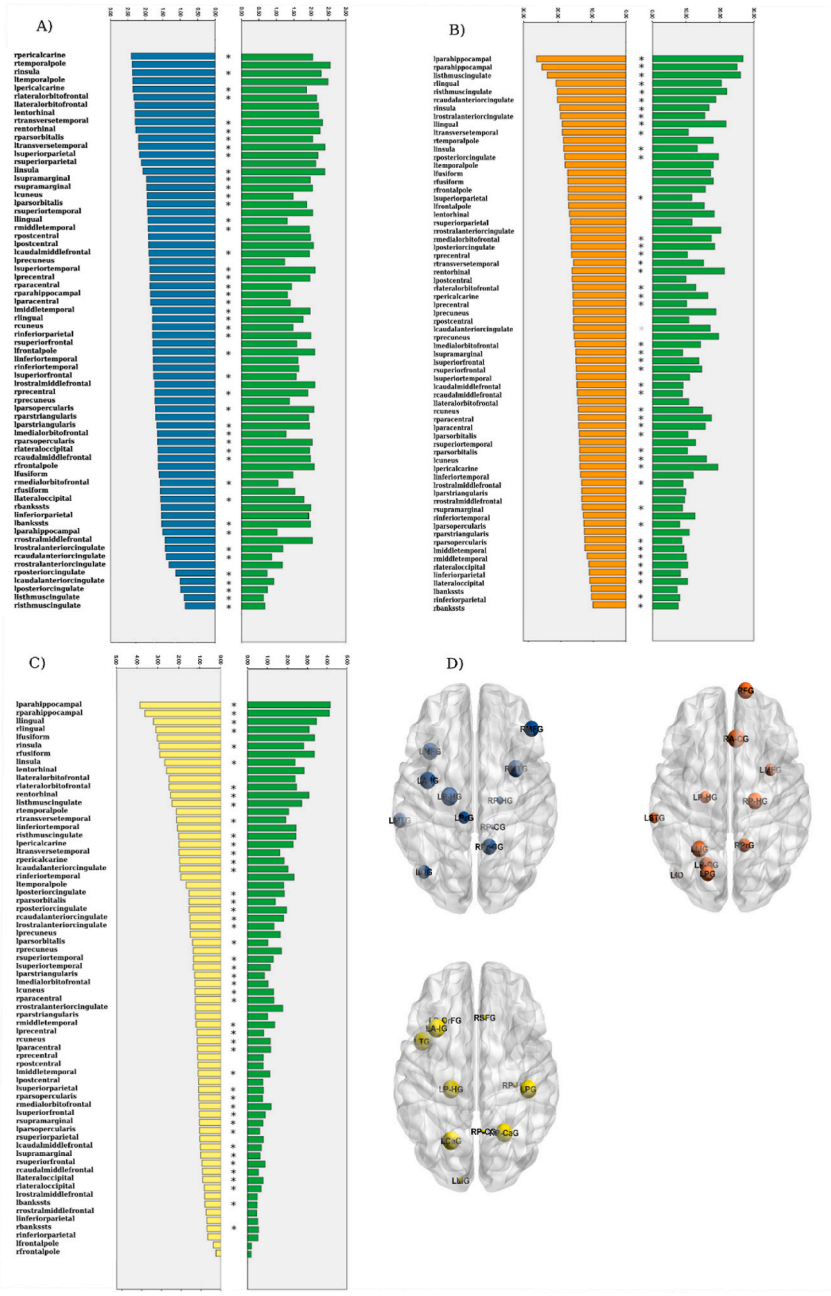

Fig. 4. Region of ROI-based analysis comparing FCD and HC for the cortical thickness (A), gyrification (B), and sulcal depth (C); (D) Brain regions exhibiting varied ROIs and statistically significant differences in the thickness, GI, and SuD.

characteristics using surface-based morphometric and machine learning to diagnose FCD [49]. Lin et al. also developed a detailed, quantitative XGBoost classifier that identified FCD type IIb using MRI and PET imaging data. Their investigation achieved 93 % sensitivity, 91 % specificity, and 9 % false-positive rates, respectively [50]. David et al. tried to improve the visual detection by using morphometric analysis of T1-weighted images [51]. They developed an artificial neural network (ANN) classifier for robust automated detection of FCDs based on these morphometric maps and probe its generalization performance in a large, independent data set.

4.5. Limitations and future works

Though our study produced good results in terms of successfully identifying aberrant clusters or regions, numerous limitations should be investigated further. First and foremost, our study employed two different kind of imaging modality (PET-MRI and PET-CT).

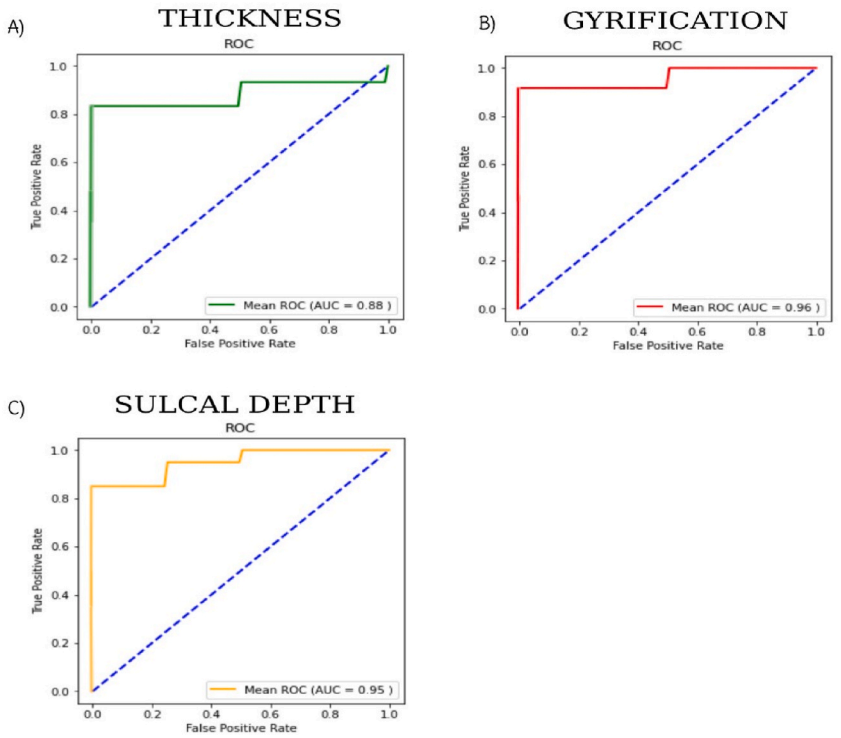

Fig. 5. Average receiver operating characteristic (ROC) curve of the SVM classifier model for the cortical thickness (A), gyrification (B), and sulcal depth (C).

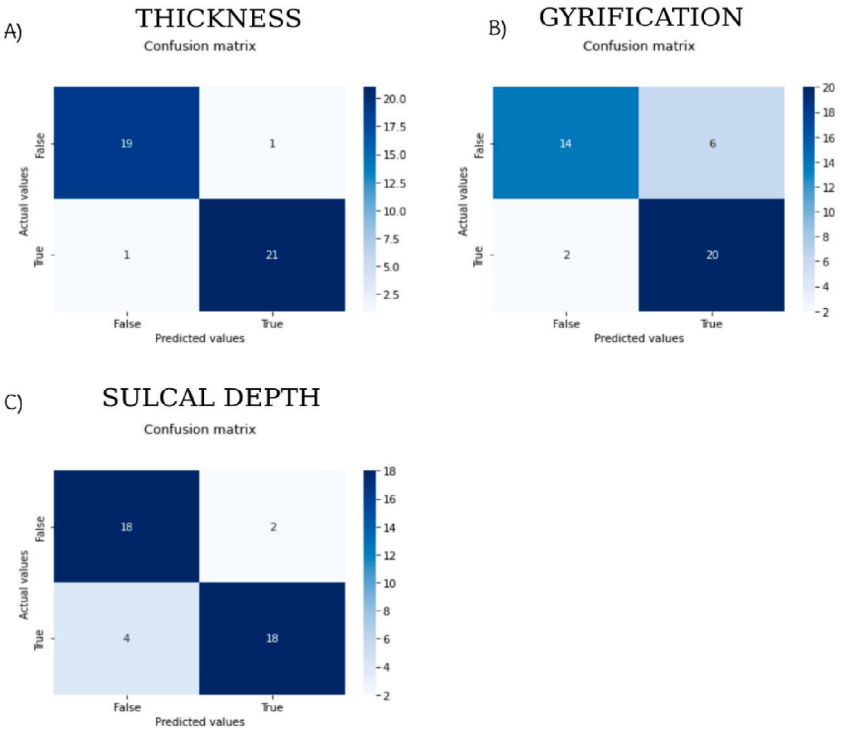

Fig. 6. Confusion matrix of the SVM classifier model for the cortical thickness (A), gyrification (B), and sulcal depth (C).

This may have a significant impact on the obtained outcome and its interpretation. While the CT component of a PET-CT scan gives anatomical information, it has significant limitations and isn't ideal for exploring the cortical surface in depth. However, PET-MRI, and more specifically the MRI component of it, is recognized and widely used for comprehensive examination of the cortical surface [52–54]. Secondly, our investigation revealed numerous anomalous clusters, which are treated by selecting the most significant cluster. Because we don't know the nature of the cluster chosen, the selection criteria have certain limits. Some of the clusters may be statistically insignificant or simply artefacts discovered during the acquisition procedures. Jacobian correction is a typical strategy for dealing with false positives [55,56], which we did not employ in our work. Thirdly, another disadvantage could be the variance issue in the brain. Our investigation did not consider age-related changes in the cortex of either group (FCD or HC). The age factor is recognized to have little effect on the sensitivity of our study [57]. Other surface analysis methodologies, such as FreeSurfer or voxel-based analysis, could be used to address the poor performance of gyrification utilising CAT12 [31,58]. Finally, the sample size is small, which can be viewed as a constraint. In machine learning, data size can be a significant issue to deal with. These difficulties are encountered in numerous machine learning analyses [59,60]. However, other approaches could be applied, such as data augmentation, which is one of the techniques used to try to improve this issue [61,62].

5. Conclusion

The cortical surfaces of the brain play a crucial role in the diagnosis of neurological diseases. The aberrant thickness, GI, and SuD in FCD patients may be associated with drug-resistant epilepsy with unmanageable seizure frequency. This study examined the critical function of brain cortical characteristics in FCD patients. thickness, GI, and SuD were assessed to identify abnormal regions. Cortical thickness appears to be the best morphological parameter for FCD diagnosis because it identified the most clusters during cluster-based analysis when compared to others. However, because surface metrics for FCD and HC may differ in many places, the contribution of sulcal depth and gyrification should be further explored. The application of machine learning to examine cortical morphological features can yield a reliable result for individual prediction of FCD.

Ethics statement

This study was approved by the Ethics Committee of Shengjing Hospital of China Medical University and the ethics approval number is 2019PS128J.

Data availability statement

In compliance with the guidelines set forth by the Ethics Committee of Shengjing Hospital of China Medical University, the datasets used in this study cannot be made publicly accessible. However, any inquiries related to accessing the datasets can be sent to Dr Han Li at leoincmu@gmail.com.

CRediT authorship contribution statement

Eric Jacob Bacon: Formal analysis, Investigation, Methodology, Validation, Writing – original draft. **Chaoyang Jin:** Data curation, Methodology, Software. **Dianning He:** Formal analysis, Resources, Software. **Shuaishuai Hu:** Data curation, Investigation, Validation. **Lanbo Wang:** Formal analysis, Validation. **Han Li:** Conceptualization, Investigation, Writing – review & editing. **Shouliang Qi:** Conceptualization, Funding acquisition, Project administration, Supervision, Writing – review & editing.

Declaration of competing interest

The authors declare that they have no known competing financial interests or personal relationships that could have appeared to influence the work reported in this paper.

Acknowledgments

The National Natural Science Foundation of China (Grant No. 82072008), the Natural Science Foundation of Liaoning Province, China (Nos. 2020-BS-049; 2021-YGJC-21), and the Fundamental Research Funds for Central Universities (Grant No. N2324004-13) supported this research.

References

[1] D.J. Englot, E.F. Chang, Rates and predictors of seizure freedom in resective epilepsy surgery: an update, Neurosurg. Rev. 37 (2014) 389–405, https://doi.org/10.1007/s10143-014-0527-9.

[2] S.H. Kim, J. Choi, Pathological classification of focal cortical dysplasia (FCD): personal comments for well understanding FCD classification, Journal of Korean Neurosurgical Societ.y 62 (3) (2019) 288–295, https://doi.org/10.3340/jkns.2019.0025.

[3] S. Jayalakshmi, S.K. Nanda, S. Vooturi, R. Vadapalli, et al., Focal cortical dysplasia and refractory epilepsy: role of multimodality imaging and outcome of surgery, Am. J. Neuroradiol. 40 (2019) 892–898, https://doi.org/10.3174/ajnr.A6041.

[4] Y.L. Tan, H. Kim, S. Lee, T. Tihan, et al., Quantitative surface analysis of combined MRI and PET enhances detection of focal cortical dysplasias, Neuroimage 166 (2018) 10–18, https://doi.org/10.1016/j.neuroimage.2017.10.065.

[5] S.J. Hong, H. Kim, D. Schrader, N. Bernasconi, et al., Automated detection of cortical dysplasia type II in MRI-negative epilepsy, Neurology 83 (2014) 48–55, https://doi.org/10.1212/WNL.0000000000000543.

[6] S.K. Kim, D.G. Na, H.S. Byun, S.E. Kim, et al., Focal cortical dysplasia: comparison of MRI and FDG-PET, J. Comput. Assist. Tomogr. 24 (2000) 296–302, https://doi.org/10.1097/00004728-200003000-00022.

[7] K. Goffin, P.W. Van, P. Dupont, K. Baete, A. Palmini, et al., Anatomy-based reconstruction of FDG-PET images with implicit partial volume correction improves detection of hypometabolic regions in patients with epilepsy due to focal cortical dysplasia diagnosed on MRI, Eur. J. Nucl. Med. Mol. Imag. 37 (2010) 1148–1155, https://doi.org/10.1007/s00259-010-1405-5.

[8] I. Sarikaya, PET studies in epilepsy, Am J Nucl Med Mol Imaging 5 (2015) 416. PMCID: PMC4620171.

[9] W.H. Hu, X. Wang, L.N. Liu, X.Q. Shao, et al., Multimodality image post-processing in detection of extratemporal MRI-negative cortical dysplasia, Front. Neurol. 9 (2018) 450, https://doi.org/10.3389/fneur.2018.00450.

[10] N. Salamon, J. Kung, S.J. Shaw, J. Koo, S. Koh, J.Y. Wu, J.T. Lerner, R. Sankar, W.D. Shields, Engel Jr., others, FDG-PET/MRI co-registration improves detection of cortical dysplasia in patients with epilepsy, Neurology 71 (2008) 1594–1601, https://doi.org/10.1212/01.wnl.0000334752.41807.2f.

[11] E.J. Bacon, C. Jin, D. He, S. Hu, et al., Epileptogenic zone localization in refractory epilepsy by FDG-PET: the comparison of SPM and SPM-CAT with different parameter Settings, Front. Neurol. 12 (2021) 1689, https://doi.org/10.3389/fneur.2021.724680.

[12] I. Sonni, S.O.H. Lesman, S.L. Baker, Iaccarino Let al, Evaluation of a visual interpretation method for tau-PET with 18F-flortaucipir. Alzheimer's & Dementia: diagnosis, Assessment & Disease Monitoring 12 (2020), e12133, https://doi.org/10.1002/dad2.12133.

[13] L. Jiang, T. Zhang, F. Lv, S. Li, et al., Structural covariance network of cortical gyrification in benign childhood epilepsy with centrotemporal spikes, Front. Neurol. 9 (2018) 10, https://doi.org/10.3389/fneur.2018.00010.

[14] T. Thesen, B.T. Quinn, C. Carlson, O. Devinsky, et al., Detection of epileptogenic cortical malformations with surface-based MRI morphometry, PLoS One 6 (2011), e16430, https://doi.org/10.1371/journal.pone.0016430.

[15] H. Spitzer, R. Mathilde, W. Kirstie, Felice Det al, Interpretable surface-based detection of focal cortical dysplasias: a Multi-Centre Epilepsy Lesion Detection study, Brain 145 (2022) 3859–3871, https://doi.org/10.1093/brain/awac224.

[16] M. Severino, A.F. Geraldo, N. Utz, D. Tortora, et al., Definitions and classification of malformations of cortical development: practical guidelines, Brain 143 (2020) 2874–2894, https://doi.org/10.1093/brain/awaa174.

[17] H.J. Yun, K. Im, J.J. Yang, U. Yoon, et al., Automated sulcal depth measurement on cortical surface reflecting geometrical properties of sulci, PLoS One 8 (2013), e55977, https://doi.org/10.1371/journal.pone.0055977.

[18] M. Li, J. Yan, H. Wen, J. Lin, et al., Cortical thickness, gyrification and sulcal depth in trigeminal neuralgia, Sci. Rep. 11 (2021) 1–9, https://doi.org/10.1038/s41598-021-95811-z.

[19] L. Pasquini, M. Scherr, M. Tahmasian, N.E. Myers, et al., Increased intrinsic activity of medial-temporal lobe subregions is associated with decreased cortical thickness of medial-parietal areas in patients with Alzheimer's disease dementia, J. Alzheim. Dis. 51 (2016) 313–326, https://doi.org/10.3233/JAD-150823.

[20] Kathryn Snyder, Emily P. Whitehead, William H. Theodore, Zaghloul, A. Kareem, Inati, J. Souheil, Sara K. Inati, Distinguishing type II focal cortical dysplasias from normal cortex: a novel normative modeling approach, Neuroimage: Clinical (30) (2021), 102565, https://doi.org/10.1016/j.nicl.2021.102565.

[21] S. Hess, B.A. Blomberg, H.J. Zhu, P.F. Høilund-Carlsen, Alavi Abass, et al "The pivotal role of FDG-PET/CT in modern medicine.", Acad. Radiol. 21 (2) (2014) 232–249, https://doi.org/10.1016/j.acra.2013.11.002.

[22] Y. Guo, H. Zhu, Z. Zhang, et al., Focal cortical dysplasia: 18F-FDG PET/CT findings and histopathologic comparisons, Eur. J. Radiol. 81 (2012) 1052–1058, https://doi.org/10.1016/j.ejrad.2011.02.006.

[23] S.E. Poirier, B.Y. Kwan, M.T. Jurkiewicz, L. Samargandy, et al., An evaluation of the diagnostic equivalence of 18F-FDG-PET between hybrid PET/MRI and PET/CT in drug-resistant epilepsy: a pilot study, Epilepsy Res. 172 (2021), 106583, https://doi.org/10.1016/j.eplepsyres.2021.106583.

[24] A. Jena, P.N. Renjen, S. Taneja, A. Gambhir, et al., Integrated 18F-fluorodeoxyglucose positron emission tomography magnetic resonance imaging (18F-FDG PET/MRI), a multimodality approach for comprehensive evaluation of dementia patients: a pictorial essay, Indian J. Radiol. Imag. 25 (2015) 342–352, https://doi.org/10.4103/0971-3026.169449.

[25] J.A. Pillai, M. Larvie, J. Chen, A. Crawford, et al., Spatial patterns of correlation between cortical amyloid and cortical thickness in a tertiary clinical population with memory deficit, Sci. Rep. 10 (2020), 20717, https://doi.org/10.1038/s41598-020-77503-2.

[26] Arnaud Marcoux, Ninon Burgos, Anne Bertrand, Marc Teichmann, Alexandre Routier, Junhao Wen, Jorge Samper-González, et al., An automated pipeline for the analysis of PET data on the cortical surface, Front. Neuroinf. 12 (2018) 94, https://doi.org/10.3389/fninf.2018.00094.

[27] S.K. Lee, S.Y. Lee, C.H. Yun, et al., The usefulness of 18F-FDG PET in the localization of epileptogenic cortex in patients with MRI positive and MRI negative focal cortical dysplasia, Seizure 14 (2005) 557–566, https://doi.org/10.1016/j.seizure.2005.09.001.

[28] F. Farokhian, I. Beheshti, D. Sone, H. Matsuda, Comparing CAT12 and VBM8 for detecting brain morphological abnormalities in temporal lobe epilepsy, Front. Neurol. 8 (2018) 428, https://doi.org/10.3389/fneur.2017.00428.

[29] I.E. Scheffer, S. Berkovic, G. Capovilla, M.B. Connolly, et al., ILAE classification of the epilepsies: position paper of the ILAE Commission for classification and Terminology, Epilepsia 21 (58) (2017) 512, https://doi.org/10.1111/epi.13709.

[30] X. Li, P.S. Morgan, J. Ashburner, J. Smith, et al., The first step for neuroimaging data analysis: DICOM to NIfTI conversion, J. Neurosci. Methods 264 (2016) 47–56, https://doi.org/10.1016/j.jneumeth.2016.03.001.

[31] R. Dahnke, R.A. Yotter, C. Gaser, Cortical thickness and central surface estimation, Neuroimage 65 (2013) 336–348, https://doi.org/10.1016/j.neuroimage.2012.09.050.

[32] R. Seiger, S. Ganger, G.S. Kranz, A. Hahn, et al., Cortical thickness estimations of FreeSurfer and the CAT12 toolbox in patients with Alzheimer's disease and healthy controls, J. Neuroimaging 28 (2018) 515–523, https://doi.org/10.1111/jon.12521.

[33] E. Luders, P.M. Thompson, K.L. Narr, A.W. Toga, et al., A curvature-based approach to estimate local gyrification on the cortical surface, Neuroimage 29 (2006) 1224–1230, https://doi.org/10.1016/j.neuroimage.2005.08.049.

[34] R. Dahnke, R.A. Yotter, C. Gaser, Cortical thickness and central surface estimation, Neuroimage 65 (2013) 336–348, https://doi.org/10.1016/j.neuroimage.2012.09.050.

[35] B. Alexander, W.Y. Loh, L.G. Matthews, A.L. Murray, et al., Desikan-Killiany-Tourville atlas compatible Version of M-CRIB neonatal parcellated whole brain atlas: the M-CRIB 2.0, Front. Neurosci. 13 (2019) 34, https://doi.org/10.3389/fnins.2019.00034.

[36] B.B. McShane, G.A. David, C.R. Gelman, L.T. Jennifer, Abandon statistical significance, Am. Statistician 73 (2019) 235–245, https://doi.org/10.1080/00031305.2018.1527253.

[37] T.T. Wong, Performance evaluation of classification algorithms by k-fold and leave-one-out cross-validation, Pattern Recogn. 48 (2015) 2839–2846, https://doi.org/10.1016/j.patcog.2015.03.009.

[38] P. Gautam, K.J. Anstey, W. Wen, P.S. Sachdev, N. Cherbuin, Cortical gyrification and its relationships with cortical volume, cortical thickness, and cognitive performance in healthy mid-life adults, Behav. Brain Res. 287 (2015) 331–339, https://doi.org/10.1016/j.bbr.2015.03.018.

[39] D. Tosun, P. Siddarth, J. Levitt, R. Caplan, Cortical thickness and sulcal depth: insights on development and psychopathology in paediatric epilepsy, BJPsych open 1 (2015) 129–135, https://doi.org/10.1192/bjpo.bp.115.001719.

[40] D.D. Jordan, A.L. Kristin, J.S. Andrew, D.S. Theodore, et al, A local group differences test for subject-level multivariate density neuroimaging outcomes, Biostatistics 22 (2021) 646–661, https://doi.org/10.1093/biostatistics/kxz058.

[41] M.E. Mayerhoefer, H.L. Prosch, D. Beer, T. Tamandl, C.H. Beyer, et al., PET/MRI versus PET/CT in oncology: a prospective single-center study of 330 examinations focusing on implications for patient management and cost considerations, Eur. J. Nucl. Med. Mol. Imag. 60 (2020) 47–51, https://doi.org/10.1007/s00259-019-04452-y.

[42] G. Varoquaux, B. Thirion, How machine learning is shaping cognitive neuroimaging, GigaScience 3 (2014), https://doi.org/10.1186/2047-217X-3-28, 2047–217X.
[43] H.M. Lee, R.S. Gill, F. Fadaie, K.H. Cho, et al., Unsupervised machine learning reveals lesional variability in focal cortical dysplasia at mesoscopic scale, Neuroimage: Clinical. 28 (2020), 102438, https://doi.org/10.1016/j.nicl.2020.102438.
[44] O. Colliot, N. Bernasconi, N. Khalili, S. Antel, Bet al, Individual voxel-based analysis of gray matter in focal cortical dysplasia, Neuroimage 29 (2006) 162–171, https://doi.org/10.1016/j.neuroimage.2005.07.021.
[45] S. Adler, K. Wagstyl, R. Gunny, L. Ronan, et al., Novel surface features for automated detection of focal cortical dysplasias in paediatric epilepsy, Neuroimage: Clinical. 14 (2017) 18–27, https://doi.org/10.1016/j.nicl.2016.12.030.
[46] B. Ahmed, C.E. Brodley, K.E. Blackmon, R. Kuzniecky, G. Barash, et al., Cortical feature analysis and machine learning improves detection of "MRI-negative" focal cortical dysplasia, Epilepsy \& Behavior 48 (2015) 21–28, https://doi.org/10.1016/j.yebeh.2015.04.055.
[47] R. Righart, P. Schmidt, R. Dahnke, V. Biberacher, et al., Volume versus surface-based cortical thickness measurements: a comparative study with healthy controls and multiple sclerosis patients, PLoS One 12 (2017), e0179590, https://doi.org/10.1371/journal.pone.0179590.
[48] M. Li, K. Hua, S. Li, C. Li, et al., Cortical morphology of chronic users of codeine-containing cough syrups: association with sulcal depth, gyrification, and cortical thickness, European radiology 29 (2019) 5901–5909, https://doi.org/10.1007/s00330-019-06165-0.
[49] T. Demerath, P.K. Christoph, H. Marcel, S. Anke, et al., Fully automated detection of focal cortical dysplasia: comparison of MPRAGE and MP2RAGE sequences, Epilepsia 63 (2022) 75–85, https://doi.org/10.1111/epi.17127.
[50] Z. Ganji, M. Hakak, Z. Aghaee, A. Seyed, et al., Automatic detection of focal cortical dysplasia type II in MRI: is the application of surface-based morphometry and machine learning Promising? Frontiers in Human Neuroscience 15 (2021) https://doi.org/10.3389/fnhum.2021.608285.
[51] Y. Lin, J. Mo, H. Jin, X. Cao, et al., Automatic analysis of integrated magnetic resonance and positron emission tomography images improves the accuracy of detection of focal cortical dysplasia type II b lesions, European Journal of Neuroscience 53 (2021) 3231–3241, https://doi.org/10.1111/ejn.15185.
[52] B. David, K.-S. Judith, S. Fabiane, W. Jan, et al., External validation of automated focal cortical dysplasia detection using morphometric analysis, Epilepsia 62 (2021) 1005–1021, https://doi.org/10.1111/epi.16853.
[53] P. Alongi, R. Laudicella, F. Panasiti, A. Stefano, et al., Radiomics analysis of brain [18F] FDG PET/CT to predict Alzheimer's disease in patients with amyloid PET positivity: a preliminary report on the application of SPM cortical segmentation, pyradiomics and machine-learning analysis, Diagnostics 12 (2022) 933, https://doi.org/10.3390/diagnostics12040933.
[54] Kazufumi Kikuchi, Osamu Togao, Koji Yamashita, Daichi Momosaka, Tomohiro Nakayama, Yoshiyuki Kitamura, Yoshitomo Kikuchi, et al., Diagnostic accuracy for the epileptogenic zone detection in focal epilepsy could be higher in FDG-PET/MRI than in FDG-PET/CT, European Radiology 31 (2021) 2915–2922, https://doi.org/10.1007/s00330-020-07389-1.
[55] S.E. Poirier, B.Y. Kwan, M.T. Jurkiewicz, L. Samargandy, M. Iacobelli, D.A. Steven, J.D. Thiessen, An evaluation of the diagnostic equivalence of 18F-FDG-PET between hybrid PET/MRI and PET/CT in drug-resistant epilepsy: a pilot study, Epilepsy Research 172 (2021), 106583, https://doi.org/10.1016/j.eplepsyres.2021.106583.
[56] S. Liu, Y. Xiong, E. Dai, J. Zhang, et al., Improving distortion correction for isotropic high-resolution 3D diffusion MRI by optimizing Jacobian modulation, Magnetic Resonance in Medicine 86 (2021) 2780–2794, https://doi.org/10.1002/mrm.28884.
[57] A.M. Fjell, L.T. Westlye, I. Amlien, T. Espeseth, et al., High consistency of regional cortical thinning in aging across multiple samples, Cerebral cortex 19 (2009) 2001–2012, https://doi.org/10.1093/cercor/bhn232.
[58] M. Schaer, M.B. Cuadra, L. Tamarit, F. Lazeyras, et al., A surface-based approach to quantify local cortical gyrification, IEEE transactions on medical imaging 27 (2008) 161–170, https://doi.org/10.1109/TMI.2007.903576.
[59] N. Madeira, J.V. Duarte, R. Martins, G.N. Costa, et al., Morphometry and gyrification in bipolar disorder and schizophrenia: a comparative MRI study, NeuroImage: Clinical. 26 (2020), 102220, https://doi.org/10.1016/j.nicl.2020.102220.
[60] A. Althnian, D. AlSaeed, H. Al-Baity, A. Samha, et al., Impact of dataset size on classification performance: an Empirical evaluation in the medical Domain, Applied Sciences 796 (11) (2021), https://doi.org/10.3390/app11020796.
[61] J. Kim, J. Kim, The impact of imbalanced training data on machine learning for author name disambiguation, Scientometrics 117 (2018) 511–526, https://doi.org/10.1007/s11192-018-2865-9.
[62] J. Wei, K. Zou, Eda, Easy Data Augmentation Techniques for Boosting Performance on Text Classification Tasks, vol. 1901, 2019, 11196, https://doi.org/10.48550/arXiv.1901.11196 arXiv preprint arXiv.